Title

Tunable Anion Exchange Membrane Conductivity and Permselectivity via Non-Covalent, Hydrogen Bond Cross-Linking

Journal

ACS Applied Materials & Interfaces, 13(44)

ISSN

1944-8244

Authors

Kingsbury, Ryan
Hegde, Maruti
Wang, Jingbo
et al.

Publication Date

2021-11-10

DOI

10.1021/acsami.1c15474

Tunable anion exchange membrane conductivity and permselectivity via non-covalent, hydrogen bond crosslinking

Ryan Kingsbury,[a] *Maruti Hegde,*[b] *Jingbo Wang,*[a] *Ahmet Kusoglu,*[c] *Wei You,*[d] *Orlando Coronell*[a*]

[a] Department of Environmental Sciences and Engineering, Gillings School of Global Public Health, The University of North Carolina at Chapel Hill, Chapel Hill, NC 27599, USA
[b] Department of Applied Physical Sciences, The University of North Carolina at Chapel Hill, Chapel Hill, NC 27599, USA
[c] Advanced Light Source, Lawrence Berkeley National Laboratory, Berkeley, CA 94720, USA
[d] Department of Chemistry, The University of North Carolina at Chapel Hill, Chapel Hill, NC 27599, USA

*Tel: 1-919-966-9010; fax: +1-919-966-7911; e-mail: coronell@unc.edu

Abstract

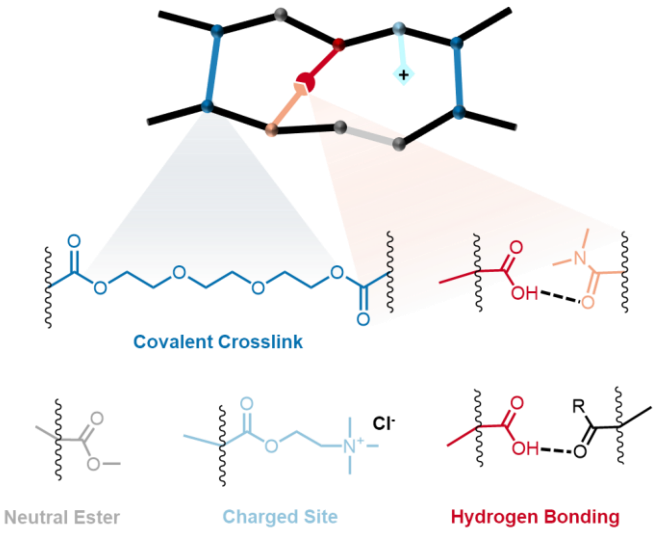

Ion exchange membranes (IEMs) are a key component of electrochemical processes that purify water, generate clean energy, and treat waste. Most conventional polymer IEMs are covalently crosslinked, which results in a challenging tradeoff relationship between two desirable properties - high permselectivity and high conductivity. In an attempt to overcome this limitation, in this work we synthesized a series of anion exchange membranes containing non-covalent crosslinks formed by a hydrogen bond donor (methacrylic acid) and a hydrogen bond acceptor (dimethylacrylamide). We show that these monomers act synergistically to improve both membrane permselectivity and conductivity relative to a control membrane without non-covalent crosslinks. Furthermore, we show that the hydrogen bond donor and acceptor loading can be used to tune permselectivity and conductivity relatively independently of one another, escaping the tradeoff observed in conventional membranes.

1.0 Introduction

Ion exchange membranes (IEMs) are a key component of electrochemical processes that purify water, generate clean energy, and treat waste.[1–6] It is desirable for IEMs to be both selective and conductive to certain ions (counter-ions), and these properties are achieved through a high concentration of charged sites covalently bound to a polymer backbone.[7–9] However, the charged hydrophilic sites cause the polymer to swell excessively in water, thus necessitating incorporation of covalent crosslinks to ensure mechanical stability.[2,9–13] The introduction of covalent crosslinks reduces the conductivity of the membrane by introducing obstacles to ion permeation,[10,11] thus imposing a challenging tradeoff between high selectivity (favored by high charge concentration) and high conductivity (favored by lower crosslinking).[14–16]

Polymer networks can also be formed using non-covalent crosslinks. Non-covalent crosslinks mediated by exchangeable bonds ("dynamic crosslinks"),[17] ionic interactions ("ionic crosslinks"),[18,19] or hydrogen bonding[20,21] can provide an alternate means of enhancing mechanical strength. Non-covalent crosslinking mechanisms have also been recognized in the renowned Nafion ion exchange membrane: physical crosslinks mediated by non-covalent interactions between its crystalline domains and ionic crosslinks between charged sites have a strong influence on its thermal and mechanical properties.[22,23] Generally speaking, non-covalent crosslinks increase the strength and toughness of polymer networks because they can break and re-form or "self-heal" in response to stress.[17–21] For example, Hu et al.[21] used non-covalent crosslinks formed by hydrogen bond donor-acceptor pairs to create a hydrogel with an impressive combination of strength, stiffness, and toughness that was unprecedented in covalently-crosslinked hydrogels. The remarkable strength of this hydrogel was attributed to the continual breaking and re-forming of hydrogen bond crosslinks within the network. Furthermore,

the hydrogels synthesized by Hu et al.[21] maintained structural integrity in aqueous solutions, which is the environment in which most IEMs operate.

Inspired by the work by Hu et al.[21], we sought to investigate whether non-covalent (hydrogen bond) crosslinking could benefit the performance of IEMs. We hypothesized that adding non-covalent (hydrogen bond) crosslinks could result in novel combinations of conductivity, selectivity, and strength that are inaccessible to conventional, covalently crosslinked membranes. For example, a transient hydrogen bond crosslink in the "broken" state might present less of an obstacle to ion conduction than a covalent crosslink, thus improving membrane conductivity without sacrificing physical integrity. In addition, hydrogen bond crosslinks may affect other relevant phenomena mediated by hydrogen bonding, such as counter-ion hydration and the balance of free vs. bound water within the membrane, that are known to play a central role in determining ion transport properties.[23–31]

Accordingly, our objective in this work was to study the effects of non-covalent crosslinking on the performance of IEMs. We synthesized anion exchange membranes incorporating methacrylic acid (MAAc) as a hydrogen bond donor and dimethylacrylamide (DMAA) as a hydrogen bond acceptor to promote non-covalent interactions within the membranes. MAAc is known to function as a proton donor, forming hydrogen bonds with acceptor moieties,[21,32] and has also been shown to exhibit strong hydrophobic interactions with ether oxygen groups (which are also present in our membranes).[32] DMAA is known to be a potent hydrogen bond acceptor.[21,33] To enable a systematic study of the influence of non-covalent crosslinks, we varied the amounts of hydrogen bond donor groups and hydrogen bond acceptor groups while maintaining an identical polymer backbone with constant charge concentration and crosslink density. We quantified membrane performance via conductivity and permselectivity measurements in sodium chloride

solutions to reflect application conditions relevant to environmental separations (e.g., electrodialysis). The effects of the hydrogen bond donor and acceptor content on water dynamics and phase-separation within the membranes were investigated via differential scanning calorimetry (DSC), atomic force microscopy (AFM), and small angle X-ray scattering (SAXS). We show that varying the loading of MAAc and DMAA in the membranes allows conductivity and permselectivity to be partially decoupled, suggesting that engineering non-covalent interactions may be a promising strategy for designing membranes that escape the permselectivity-conductivity tradeoff.

2.0 Results and Discussion

2.1 Anion exchange membranes with non-covalent crosslinking moieties

Membranes in this study contained three groups of monomers (Figure 1): 1) covalent crosslinker poly(ethylene glycol) diacrylate or PEGDA (at molar ratio X); 2) neutral ester (methyl methacrylate or MMA), hydrogen bond donor (methacrylic acid or MAAc), and/or hydrogen bond acceptor (N,N-dimethylacrylamide or DMAA, all of which are monoacrylates (at total molar ratio Y); and 3) cationic charged group [(methacryloyloxy)ethyl]trimethylammonium chloride or MAOTMAC (at molar ratio Z). The molar ratios of these three components were kept fixed in all membranes (X: Y: Z = 1.2: 1: 1). Only the relative amounts of hydrogen bond donor (MAAc), hydrogen bond acceptor (DMAA), and neutral ester (MMA) were varied, keeping the total molar ratio Y fixed. Note that by design, all membranes share an identical C-C backbone with C=O groups immediately adjacent to the backbone. All membranes also have the same fixed charge concentration (i.e., ion exchange capacity, determined by the Z value) and crosslinking density.

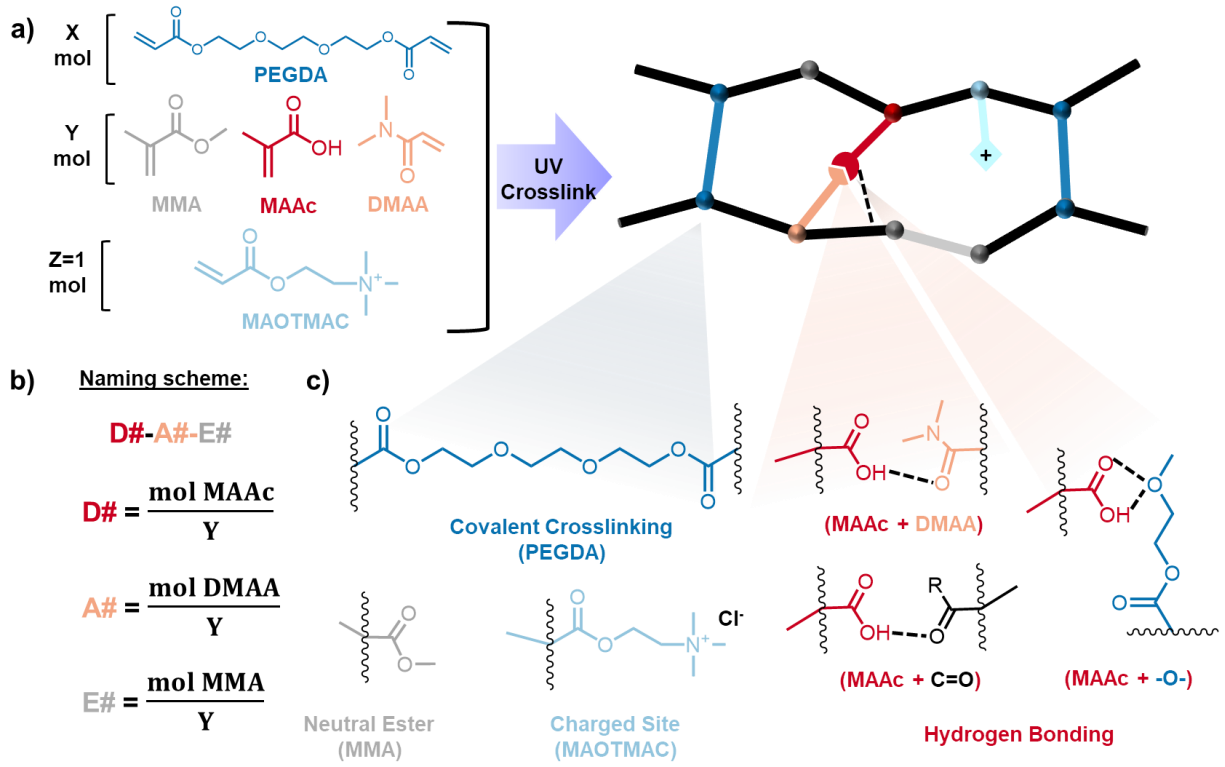

Figure 1. Synthesis of anion exchange membranes with physical crosslinks mediated by hydrogen bonding. a) Photocrosslinkable monomers; b) Membrane naming scheme; c) Functions of the various monomers. PEGDA is the covalent crosslinker, MMA is the neutral ester, MAAc is the hydrogen bond donor, DMAA is the hydrogen bond acceptor, and MAOTMAC is the cationic monomer. A molar ratio X:Y:Z = 1.2:1:1 was used in the fabrication of all membranes.

The molar compositions of all membranes prepared in this study are listed in Table 1. Each membrane was designated D#-A#-E#, where the #s following D, A, and E represent the molar percentages of Y occupied by hydrogen bond donor, acceptor, and neutral ester, respectively. Thus, in membrane D25-A25-E50, MAAc (donor) and DMAA (acceptor) each comprise 25% of total monoacrylates (Y) and MMA (neutral ester) comprises the remaining 50%. After UV-initiated photopolymerization, all compositions listed in Table 1 formed flexible, freestanding membranes that were optically clear immediately after synthesis, and became translucent and somewhat cloudy upon immersion in water. Photographs illustrating this behavior are provided in the Supporting Information. The cloudiness that we observed may indicate nanoscale phase-

separation within the polymer,[34,35] and is a topic we explore further in a later section. The gel fraction of the membranes we prepared ranged from 81-86%, with an average value of 84% (Table 1), indicating that the majority of the monomers in our mixtures were incorporated into the crosslinked polymer network.

FTIR spectra of the dry membranes (Figure 2) further confirmed that hydrogen bond donor (MAAc) and hydrogen bond acceptor (DMAA) monomers were incorporated into the polymer structure. Individual monomer spectra, shown in the Supporting Information, revealed a distinctive peak at 1690 cm^{-1} for MAAc, characteristic of C=O stretching in unsaturated carboxylic acids.[36] DMAA exhibited two distinctive peaks at 1647 cm^{-1} and 1610 cm^{-1}. The first is characteristic of C=O stretching in tertiary amides,[36] while the origin of the second peak is not clear. PEGDA (crosslinker), MAOTMAC (charged monomer), and MMA (neutral ester) all displayed a strong peak at ~1720 cm^{-1}, which corresponds to C=O stretching in unsaturated esters.[36–40] In addition, MAOTMAC showed a strong, sharp peak at 956 cm^{-1}, which is characteristic of the quaternary ammonium headgroup.[41]

The incorporation of MAAc into membranes was indicated by the broadening of the ~1720 cm^{-1} peak towards lower frequencies, reflecting the combination of C=O stretching from the unsaturated esters (1720 cm^{-1}) and the carboxylic acid (1690 cm^{-1}). The presence of DMAA in the membranes resulted in the emergence of an additional peak between 1647 cm^{-1} and 1610 cm^{-1} that was not visible in membranes without DMAA. This peak is associated with the amide group.[42] All membranes exhibited a strong, sharp peak at 956 cm^{-1}, confirming incorporation of the MAOTMAC monomer,[41] and weak, broad peaks in the O-H stretching (3200-3400 cm^{-1}) region normally associated with hydrogen bonding.[36] The lack of a stronger signal in this region may be a consequence of the fact that the membranes were scanned in the dry state.

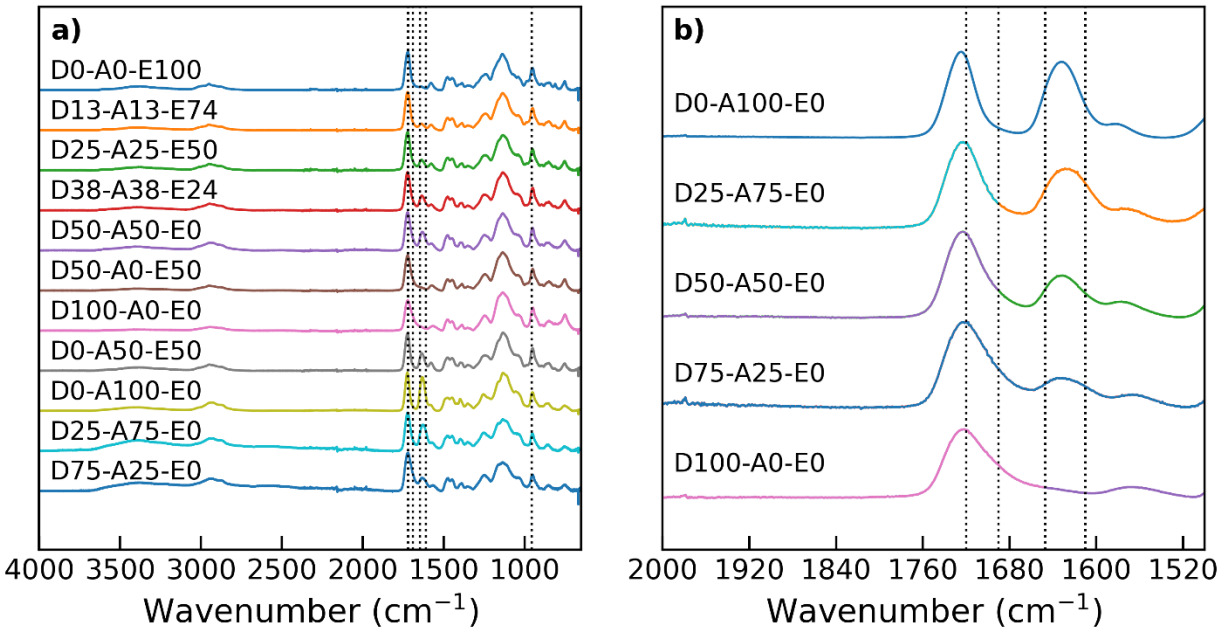

Figure 2. FTIR spectra of synthesized anion exchange membranes. a) Complete spectra of all membranes. Vertical lines are placed at 1720 cm^{-1} (C=O stretch in PEGDA, MMA, MAOTMAC), 1690 cm^{-1} (C=O stretch in MAAc), 1647 cm^{-1} (C=O stretch in DMAA), 1610 cm^{-1} (unidentified peak associated with DMAA), and 956 cm^{-1} (quaternary ammonium headgroups in MAOTMAC). b) Detail of the C=O stretching region for a subset of the membranes. In this subset, the proportion of MAAc:DMAA is varied from 0 to 1 (these membranes contain no MMA). The incorporation of MAAc (hydrogen bond donor) in the membranes can be seen in the broadening of the peak at ~1720 cm^{-1} toward lower wavenumbers; incorporation of DMAA is shown by the emergence of a peak between 1647 cm^{-1} and 1610 cm^{-1}. Peak positions were identified via spectra of individual monomers and binary mixtures containing only two monomers (see Supporting Information).

2.2 Permselectivity, Conductivity, and Water Uptake Properties

2.2.1 Performance of membranes containing only donor or acceptor

To evaluate the effects of non-covalent crosslinking by the hydrogen bond donor (MAAc) and hydrogen bond acceptor (DMAA) on membrane performance, we first consider membranes in which MAAc and DMAA were added individually, relative to the control membrane D0-A0-E100 which contained neither donor nor acceptor. Neutral ester (MMA) was substituted with MAAc or DMAA to various degrees, such that the total monoacrylate content of every membrane remained constant (Y=1; see Table 1). As noted in the Introduction, in addition to

donating protons to form hydrogen bonds, MAAc is also known to form interpolymer complexes with ether oxygen groups (e.g., on PEGDA),[21,32] which is another mechanism by which MAAC may promote non-covalent crosslinking. The water uptake, conductivity, and permselectivity of these membranes are summarized in Figure 3. Focusing first on water uptake, Figures 3a and 3b show clearly that adding MAAc to the membranes reduced their water uptake relative to the control membrane, while adding DMAA increased it. Since the carboxyl and acrylamide groups on MAAc and DMAA, respectively, are both more hydrophilic than the methyl group on MMA, which is the only monoacrylate present in the control membrane, one would expect addition of either MAAc or DMAA to increase water uptake. The fact that adding MAAc decreased water uptake suggests that MAAc was not hydrogen bonding with water molecules, which would presumably cause additional water uptake. Instead, MAAc may have formed hydrogen bonds with other carbonyl groups on the polymer. Since the C=O groups are all located immediately adjacent to the polymer backbone (see Figure 1), hydrogen bonding with MAAc would have the effect of pulling adjacent polymer chains closer together since the O-H-O hydrogen bond would be much shorter than the length of the PEGDA crosslinker. It is also possible that hydrogen bonding between MAAc and ether oxygen groups on the PEGDA crosslinker resulted in interpolymer complexes which would have a similar effect of pulling polymer chains closer together. Such complexes, arising from hydrogen bonding and further stabilized by strong hydrophobic effects (i.e., structuring of water around the COOH-O moieties), have been shown to form between the polymer analog of MAAc—poly(methacrylic acid) or PMAA—and PEG.[32]

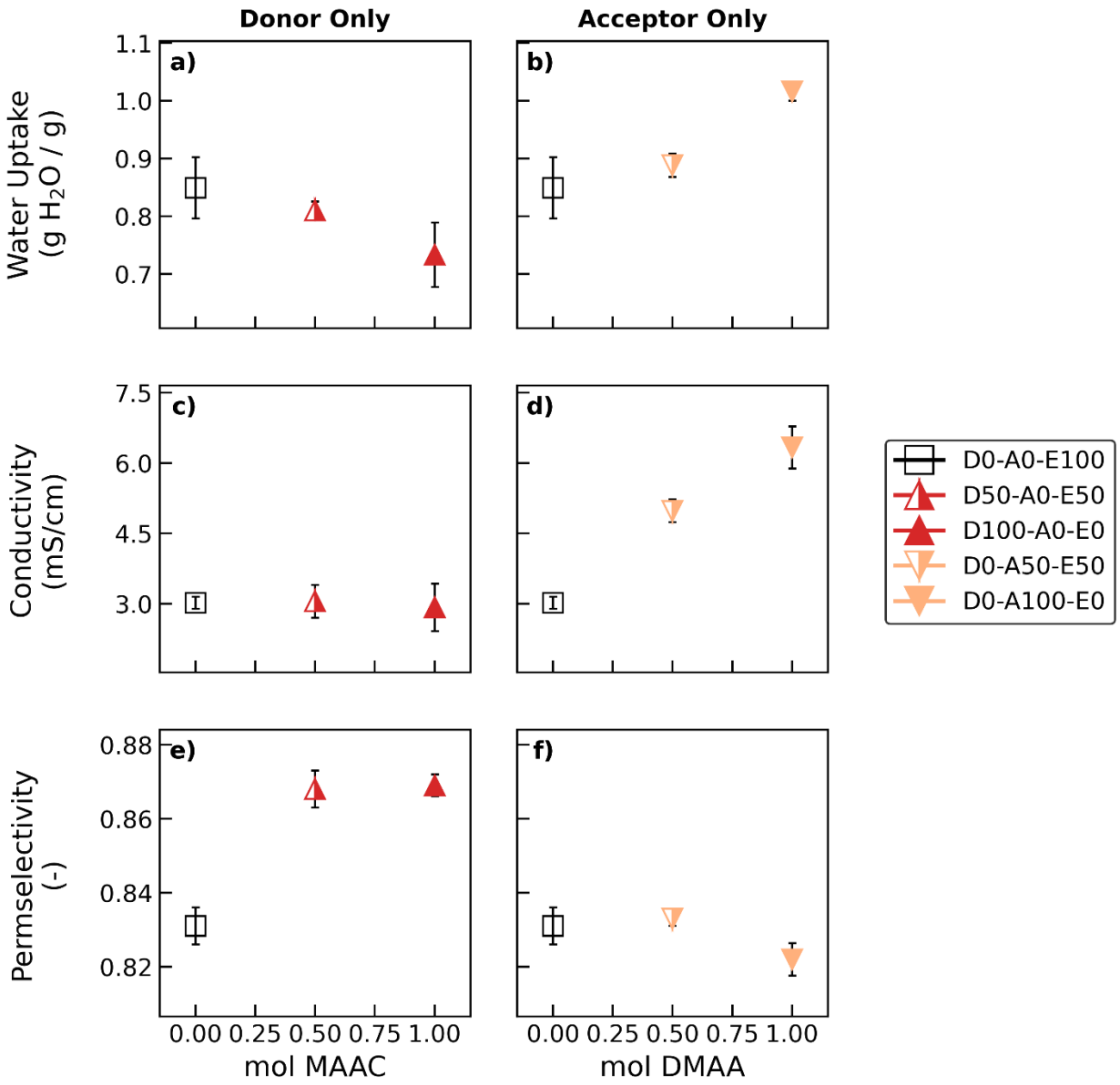

Figure 3. Membrane water uptake (a,b), conductivity (c,d), and permselectivity (e,f) vs. hydrogen bond donor (i.e., MAAc) or acceptor (i.e., DMAA) content for membranes containing only MAAc (left column) or DMAA (right column). Refer to the legend and Table 1 for the full composition of the membrane represented by each data point. For all membranes shown, the total mol of hydrogen bond donor (MAAc) + acceptor (DMAA) + neutral ester (MMA) was fixed at Y=1 mol; see Figure 1 and Table 1). Red color corresponds to hydrogen bond donor (MAAc), and peach color corresponds to hydrogen bond acceptor (DMAA). Error bars represent the standard error of at least five replicate measurements.

Figures 3c and 3d illustrate the effects of hydrogen bond donor and acceptor, respectively, on conductivity. It is striking that adding donor (MAAc) to the membrane did not result in any

substantial change in conductivity (Figure 3c), even though water uptake was reduced. In most IEMs, decreasing water uptake is expected to reduce the conductivity.[16,43] In contrast to MAAc, the hydrogen bond acceptor (DMAA) increased conductivity relative to the control membrane (Figure 3d), which is what would be expected from the observed increase in water uptake (Figure 3b).

A contrast in behavior between MAAc and DMAA is also evident in the plots of membrane permselectivity. Figure 3e shows that adding MAAc to the membranes substantially increased permselectivity, and this effect was not linear with the MAAc loading: the membrane containing 0.5 mol MAAc had almost the same permselectivity as the membrane containing 1.0 mol MAAc, and both were substantially higher than that of the control membrane containing only MMA. In contrast, DMAA had only a minor effect on permselectivity (Figure 3f). At 0.5 mol loading, the permselectivity was roughly equal to that of the control membrane, while at 1.0 mol loading, the permselectivity was slightly lower. The higher permselectivity of MAAc-containing membranes may be related to the reduction in water uptake presumably caused by non-covalent interactions between MAAc and carbonyl or ether oxygen groups, as discussed above.

Overall, addition of a hydrogen bond donor (MAAc) resulted in a decrease in water uptake and increase in permselectivity, but no change in conductivity. Addition of a hydrogen bond acceptor (DMAA) resulted in an increase in water uptake and substantial increase in conductivity, but only a slight decrease in permselectivity. Therefore, our results indicate that addition of hydrogen bond donors and/or acceptors may enable tuning relatively independently conductivity and permselectivity and therefore escaping the conductivity-permselectivity tradeoff typically observed in ion exchange membranes.

2.2.2 Performance of membranes containing both donor and acceptor

We next consider the water uptake, conductivity, and permselectivity of the membranes containing both donor and acceptor, which are summarized in Figure 4. Two series of membranes are shown. In the first series (left column), hydrogen bond donor and acceptor (MAAc and DMAA, respectively) were introduced in a 1:1 ratio under the assumption that each donor-acceptor pair would form a single non-covalent crosslink (see Figure 1c). In this series, the neutral ester (MMA) was progressively replaced by equal amounts of donor and acceptor, such that the total monoacrylate content of every membrane remained constant (Y=1; see Table 1). As such, the last membrane in the series (D50-A50-E0) contained 0.5 mol each of donor and acceptor, and 0 mol MMA. In the second series (right column), we held the total loading of donor + acceptor constant at Y=1 mol (with 0 mol MMA) and varied the donor/acceptor ratio. Thus, the monoacrylate content of this subset of membranes varied from 0 mol acceptor: 1 mol donor to 1 mol donor : 0 mol acceptor, and none contained neutral ester (MMA).

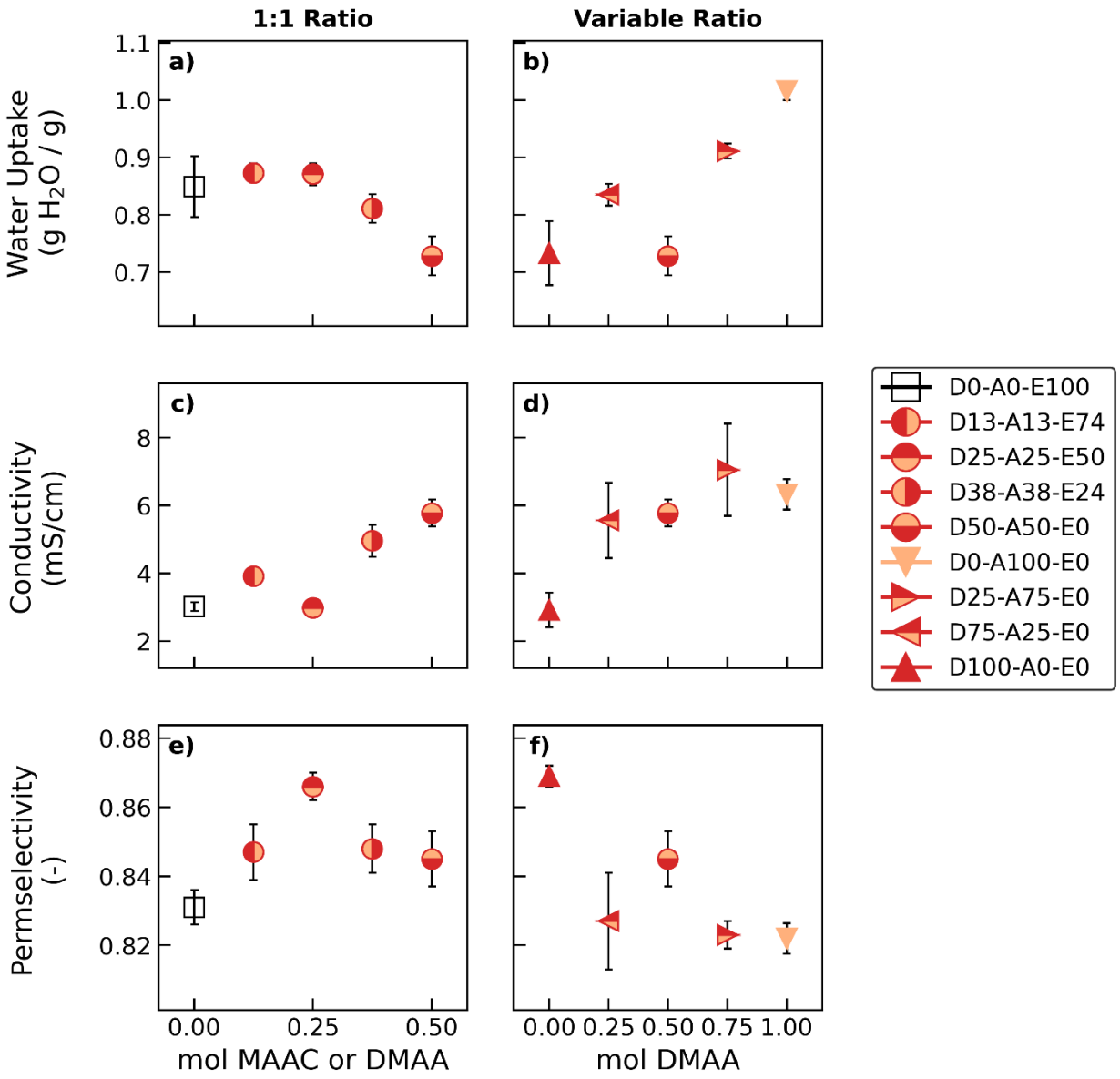

Figure 4. Membrane water uptake (a,b), conductivity (c,d), and permselectivity (e,f) of membranes containing variable amounts of hydrogen bond donor (i.e., MAAc) and acceptor (i.e., DMAA). The left column (a,c,e) shows membranes in which donor and acceptor were added in a 1:1 ratio, while the right column (b,d,f) shows membranes in which the ratio of donor to acceptor was varied. Refer to the legend and Table 1 for the composition of the membrane represented by each data point. For all membranes shown, the total mol of crosslinker PEGDA (X), monoacrylates (Y), and charged monomer MAOTMAC (Z) are fixed (X=1.2 mol, Y=1 mol, Z=1 mol; see Figure 1 and Table 1). Some membranes appear in both columns. Red color corresponds to hydrogen bond donor (MAAc), and peach color corresponds to hydrogen bond acceptor (DMAA). Error bars represent the standard error of at least five replicate measurements.

Focusing first on water uptake, we see in Figure 4a that when donor and acceptor were added in a 1:1 ratio, water uptake increased slightly compared to the control membrane, before decreasing substantially as the total donor+acceptor loading approached 1 mol. With a variable donor/acceptor ratio (Figure 4b), water uptake generally increased relative to the control membrane as the proportion of acceptor increased, although membrane D50-A50-E0 was an exception. Confirming what was observed when the donor (MAAc) was added by itself (Figure 3a), Figure 4b suggests that MAAc reduced water uptake. This result could be explained by hydrogen bonding between MAAc-DMAA or by non-covalent interactions between MAAc and other carbonyl or ether oxygen groups (see Figure 1c), any of which may create non-covalent crosslinks that help counteract the swelling pressure in the membrane. By contrast, hydrogen bond acceptor (DMAA) appears to increase the water uptake, as indicated by the fact that membrane D0-A100-E0 (containing DMAA without MAAc or MMA) had the highest water uptake of any membrane shown.

This can be explained by considering that the DMAA molecule is more hydrophilic than MMA, but (unlike MAAc) lacks the ability to form hydrogen bonds in the absence of a proton donor. Thus, the non-monotonic dependence of water uptake on donor:acceptor loading in Figure 4a can be interpreted as the result of competitive effects of the donor and acceptor: at higher donor loadings, the tendency of MAAc to reduce water uptake outweighs the tendency of DMAA to increase it.

It is interesting to compare the individual effects of the donor and acceptor to their combined effect on water uptake. By itself, the donor (MAAc) had a smaller effect on water uptake than the acceptor (DMAA): the *decrease* in water uptake between the control membrane and D100-A0-E0 (0.116 g H_2O per g, corresponding to maximum MAAc content) was smaller than the

increase in water uptake between the control membrane D0-A0-E100 and D0-A100-E0 (0.167 g H_2O per g, corresponding to maximum DMAA content). Nevertheless, adding MAAc and DMAA in a 1:1 ratio (D50-A50-E0) had as net effect a *reduction* of the water uptake by 0.1~~039~~21 g H_2O per g compared to the control membrane (Figure 4a). Thus, the combined effects of MAAc and DMAA on water uptake were not additive. This observation is consistent with the presence of non-covalent, hydrogen-bonded crosslinks between the two monomers: acrylamide moieties on DMAA that are bonded to MAAc are not free to interact with water, so their ability to increase membrane water uptake is suppressed. If the carboxyl and acrylamide moieties in the -D50-A50-E0 membrane were unbonded, the combined effects of MAAc and DMAA should have been roughly additive, and the water uptake of the D50-A50-E0 membrane would have increased.

Membrane conductivity increased in a roughly linear fashion relative to the control membrane as hydrogen bond donor and acceptor were added to the membrane in a 1:1 ratio (Figure 4c). As was the case when MAAc was added by itself (Figures 3a and 3c), this result was contrary to expectations considering that adding donor and acceptor also reduced the water uptake (Figure 4a). Normally, reducing the water uptake would be expected to reduce the conductivity, and vice-versa.[16,43] On the other hand, the expected relationship between water uptake and conductivity is exhibited by the series of membranes in Figure 4d, where increasing the proportion of hydrogen bond acceptor (DMAA) increased both water uptake and conductivity. A possible explanation for these observations is that when MAAc is present by itself or in excess (i.e., without a sufficient number of DMAA hydrogen bond acceptors to pair with), its -COOH group ionizes to $-COO^-$ and repels chloride counter-ions. Previous studies[44–47] have shown that some -COOH groups inside of polyamide reverse osmosis membranes dissociate with pK_a ~ 5.4,

lower than the neutral pH solutions used here. Repelling counter-ions from the polymer may reduce intrapore energy barriers and lead to higher conductivity.[48]

The combined effects of donor and acceptor on permselectivity are shown in Figures 4e and 4f. Adding donor and acceptor in a 1:1 ratio always improved membrane permselectivity relative to the control membrane (0.854-0.866 vs. 0.831; Figure 4e); however, permselectivity did not increase monotonically with donor and acceptor concentration. Surprisingly, the membrane with the highest permselectivity (D25-A25-E0) had a water uptake that was slightly higher than that of the control membrane (0.871 vs. 0.849 g H_2O g^{-1}; Figure 3a). In general, permselectivity is expected to decrease with increasing water uptake,[16] contrary to observations in Figure 4e, so once again introduction of donor and acceptor in a 1:1 ratio resulted in novel behavior in these membranes. In Figure 4f, we see that membrane D100-A0-E0, which contained no hydrogen bond acceptor (DMAA), had the highest permselectivity of all (0.869) and that increasing the proportion of acceptor generally reduced the permselectivity, consistent with Figure 3f.

Altogether, Figures 3 and 4 illustrate that certain combinations of donor and acceptor resulted in novel changes in membrane properties (e.g., decreases in water uptake accompanied by increases in conductivity) that defied expectations based on known tradeoff relationships. The hydrogen bond donor (MAAc) and acceptor (DMAA) exhibited contrasting behavior with respect to their effects on water uptake, conductivity, and permselectivity. Specifically, MAAc reduced water uptake and increased permselectivity without affecting conductivity (Figure 3c, 3e), while DMAA increased water uptake and conductivity without substantially decreasing permselectivity (Figure 3d, 3f). Furthermore, the effects of MAAc and DMAA when added together (Figure 4) were not an additive combination of their individual effects (Figure 3).

The combined effects of donor, acceptor, and neutral ester on membrane conductivity and permselectivity are summarized in Figure 5, which presents contour plots of each property as a function of the fractional monoacrylate composition (Y). Figure 5 illustrates clearly that MAAc-containing membranes (left edge) exhibit high permselectivity, while DMAA-containing membranes (lower right vertex) exhibit higher conductivity.

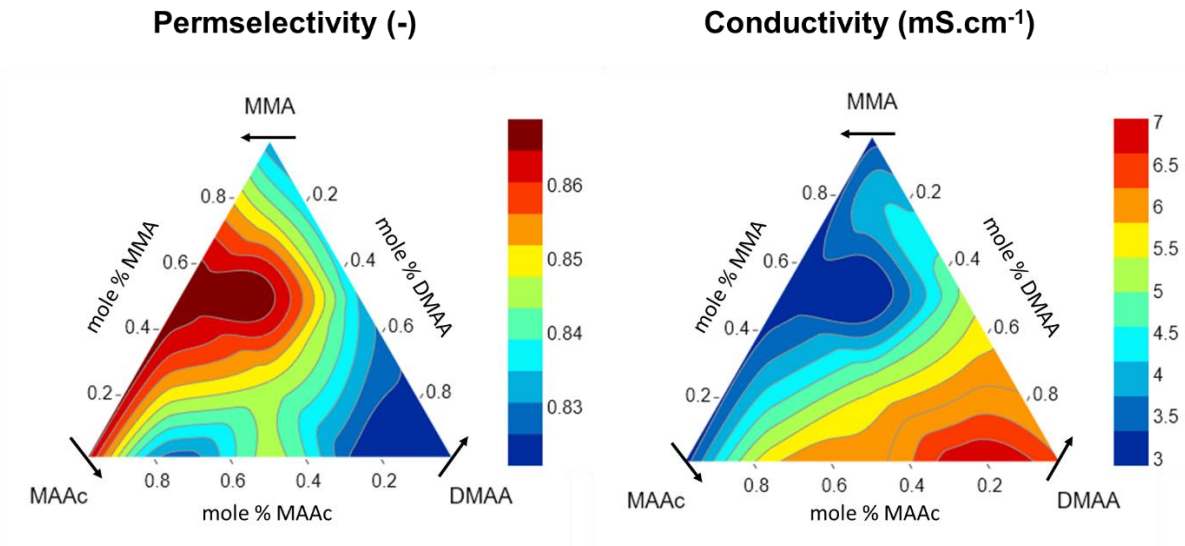

Figure 5. Fractional monoacrylate (MMA, MAAc, or DMAA) composition vs. permselectivity (left) and conductivity (right) for all membranes in this work. The fractional composition at a particular location within the plot is determined by reading the axis value in the direction indicated by the arrow next to each component. For example, horizontal lines correspond to different fractional amounts of MMA (neutral ester), which are labeled on the left axis. Downward-sloping lines at -60° from the horizontal correspond to different amounts of MAAc (donor), which are labeled on the bottom axis. Upward-sloping lines at 60° from the horizontal correspond to different amounts of DMAA (acceptor), which are labeled on the right axis. The vertices of each plot represent membranes that contain only MMA, MAAc, or DMAA in the monoacrylate block (e.g., membrane D100-A0-E0 is the lower left vertex).

2.2.3 Permselectivity-conductivity tradeoff in membranes containing donor and acceptor

The unusual effects of donor and/or acceptor addition described in Sections 2.2.1 (Figure 3) and 2.2.2 (Figure 4) appear to allow MAAc and DMAA to be used to tune conductivity and permselectivity somewhat independently of water uptake. For example, consider membranes D100-A0-E0 (solid red triangle) and D50-A50-E0 (half-filled circle). The difference between the

two membranes is that membrane D100-A0-E0 contained no hydrogen bond acceptor, while membrane D50-A50-E0 contained 0.5 mol each of donor and acceptor. Both had essentially the same water uptake (~0.73 g H_2O per g; Figure 4a and 4b), but the D50-A50-E0 membrane had roughly twice the conductivity of the D100-A0-E0 membrane (5.78 $mS.cm^{-1}$ vs. 2.92 $mS.cm^{-1}$), while the D100-A0-E0 membrane had higher permselectivity (0.869 vs. 0.845). Thus, replacing some of the hydrogen bond donor (MAAc) with hydrogen bond acceptor (DMAA) substantially increased the conductivity of the membrane without changing its water uptake and only slightly decreasing its permselectivity. Plots of conductivity and permselectivity vs. water uptake for all membranes are provided in the Supporting Information to further illustrate this tunability.

The permselectivity and conductivity tradeoff exhibited by all membranes is summarized in Figure 6, which shows that altogether, the membranes exhibited a tradeoff between high permselectivity and high conductivity, similar to that observed in conventional IEMs.[14–16] However, all membranes containing hydrogen bond donor (MAAc) or acceptor (DMAA) had higher performance (i.e., were closer to the upper right corner of the plot, corresponding to high selectivity and conductivity), than the control membrane which contained neither. Moreover, there is a general trend, visible by examining the symbol colors, that membranes containing more MAAc tended to have higher permselectivity / lower conductivity, while membranes containing more DMAA tended to have higher conductivity / lower permselectivity, as illustrated previously in Figure 5. Thus, manipulating the MAAc and DMAA content in these membranes provides a means of navigating along the tradeoff frontier to optimize for one property or the other, and their combined inclusion can be used to improve permselectivity and conductivity simultaneously compared with the control membrane.

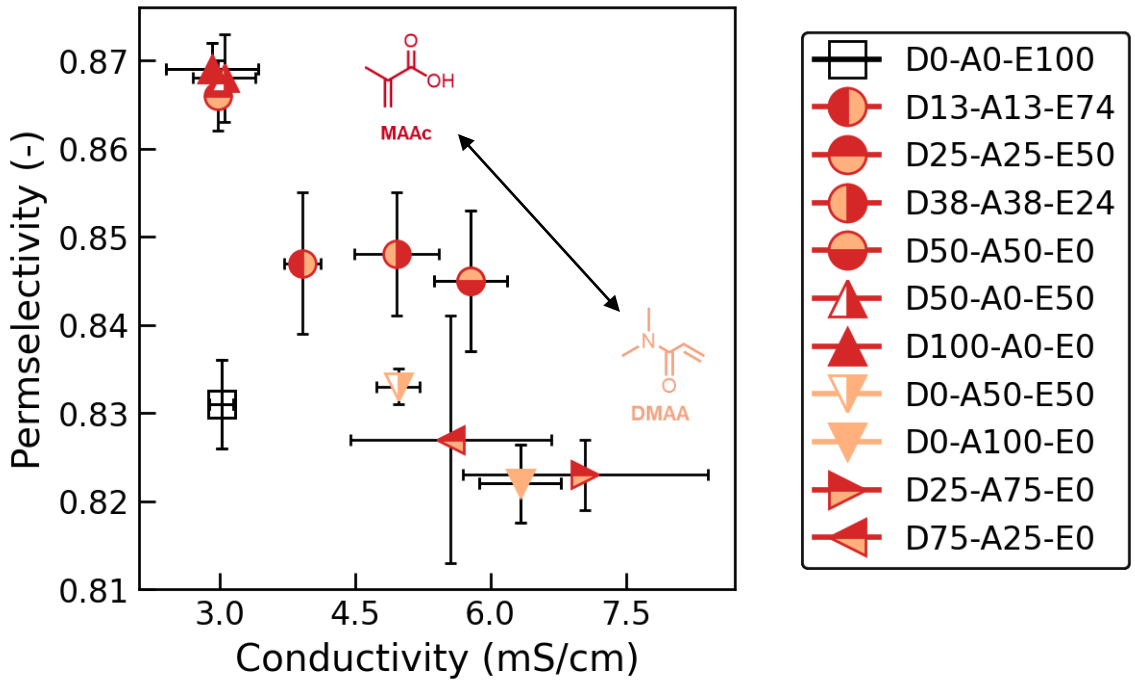

Figure 6. Membrane permselectivity vs. conductivity for all membranes in this work. Error bars represent the standard error of at least five replicate measurements. Refer to the legend and Table 1 for the composition of the membrane represented by each data point. Red color corresponds to hydrogen bond donor (MAAc), and peach color corresponds to hydrogen bond acceptor (DMAA). Error bars represent the standard error of at least five replicate measurements.

2.2.4 State-of-water analysis

To gain a more fundamental understanding of how MAAc and DMAA affected membrane water uptake, we examined the state of water in the membranes. Three populations of water molecules are generally observed inside charged polymer membranes—"free" water that behaves similarly to bulk water, "bound" or "non-freezable" water that is strongly associated with the polymer or ions, and "weakly bound" water in an intermediate state.[24,49–51] For the membranes studied here, the fractions of total water uptake attributable to bound water ranged from 70-98%, and were in a similar range to the bound water fractions of other methacrylate-based membranes reported in literature.[24,52] Hence, the majority of the water absorbed by our membranes was strongly associated with the polymer.

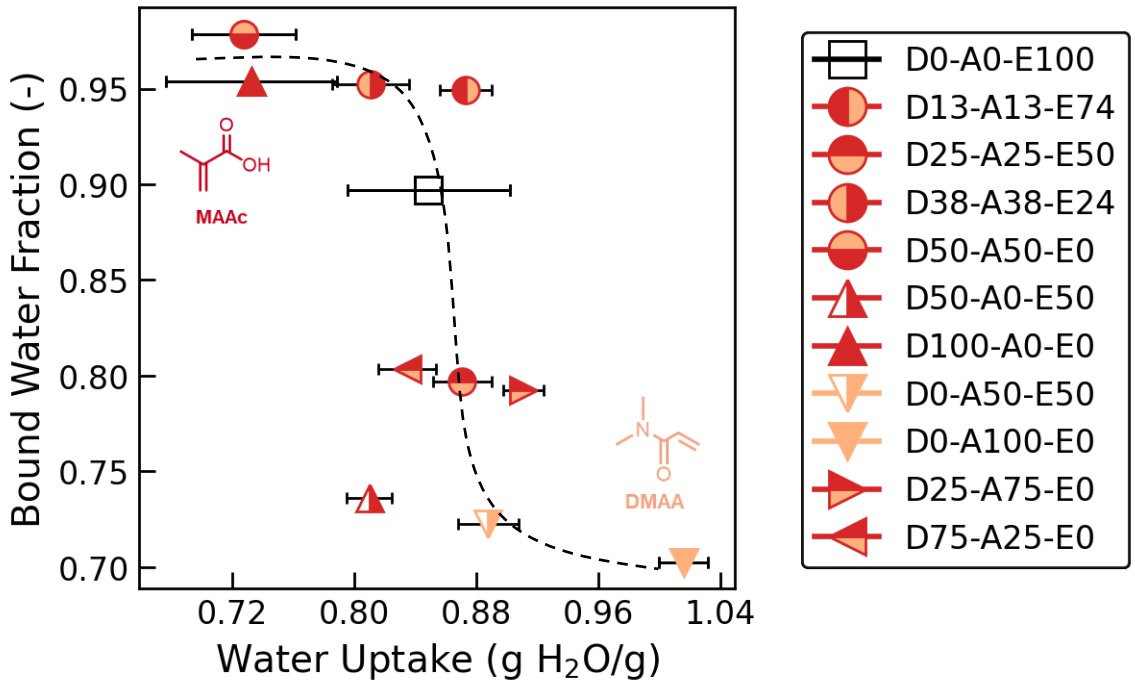

Figure 7. Membrane bound (non-freezable) water fraction vs. total water uptake. Refer to the legend and Table 1 for the composition of the membrane represented by each data point. Red color corresponds to hydrogen bond donor (MAAc) and peach color corresponds to hydrogen bond acceptor (DMAA). The dashed curve is shown to guide the eye.

Figure 7 presents the relationship between the bound water fraction and the total water uptake for all membranes studied. Overall, the plot resembles a sigmoid shape in which higher fractions of bound water (relative to the control membrane) are associated with lower total water uptake, while lower fractions of bound water are associated with higher total water uptake. There are four membranes with a higher bound water fraction than the control membrane (~0.95 vs 0.90), and all of these contain either 1) donor without acceptor (e.g., D100-A0-E0, red triangle) or 2) donor and acceptor in a 1:1 ratio. The remaining six membranes have a substantially lower bound water fraction than the control (0.70 – 0.80). Among these six, four contain either 1) acceptor without donor (e.g., D0-A100-E0, peach triangle) or 2) donor and acceptor in an unequal ratio.

Based on this rough classification, we may hypothesize that hydrogen bond donor (MAAc) generally increases the bound water fraction by 1) reducing the space between adjacent polymer chains via non-covalent crosslinking with various moieties on the membranes, as illustrated in Figure 1c, 2) forming complexes with ether oxygen groups on the PEGDA crosslinker that bind water via hydrophobic effects,[32] or 3) by directly bonding with water molecules since, by definition, bound water interacts strongly via electrostatic or hydrogen bonding with the polymer structure.[50] However, the fact that MAAc caused a decrease in total water uptake (see Section 2.2.1) suggests that direct MAAc-water hydrogen bonding is unlikely, since MAAc-water hydrogen bonding would likely have increased water uptake. In contrast, hydrophilic DMAA lowers the bound water fraction by attracting additional free water molecules, increasing the overall water content of the membrane. Furthermore, the effects of donor and acceptor on bound water fraction are clearly non-additive, as was the case with total water uptake (see Section 2.2.2).

To further evaluate whether the MAAc interacted directly with water in the membranes, we carried out pH-dependent swelling tests on selected membranes (see Supporting Information). We did not observe any dimensional changes when the membranes were exposed to pH 3, 9, or 11, indicating either that the -COOH groups on MAAc were entirely inaccessible to the aqueous phase (which would prevent them from deprotonating at high pH), or that the covalent crosslinks in the membranes were sufficiently strong to resist any increases in the swelling pressure caused by the breaking of non-covalent crosslinks due to -COOH deprotonation.

Together, the total water uptake (Section 2.2.1, 2.2.2) and bound water uptake (this section) results provide evidence that DMAA interacts directly with water molecules in the membrane, thereby increasing water uptake in linear fashion with DMAA loading (Figure 3b), while MAAc

generally does not (Figure 3a) presumably because its hydrogen bond capacity is used for non-covalent crosslinking with DMAA or other moieties.

2.3 Phase separation in the membrane

The hypothesis that MAAc does not interact directly with sorbed water molecules is consistent with an observation of Hu et al.[21] that hydrogels containing MAAc and DMAA formed hydrophobic clusters which allowed the MAAc and DMAA to remain hydrogen bonded (and therefore to not interact with water) even when the gel was immersed in aqueous solution. The lack of dimensional changes with pH and the cloudy appearance of our membranes when hydrated (see Section 2.1) are additional signs consistent with the presence of micro- or nanoscopic phase separation.[34,35] To investigate this possibility further, we performed phase-contrast atomic force microscopy (AFM) on a subset of the membranes studied. Although the images showed contrasts indicative of sub-micron phase separation, the presence of hydrogen bond donor or acceptor did not appear to cause systematic changes in phase separation compared to the control membrane (see Figure S7). We also obtained SAXS profiles of membranes D0-A0-E100, D100-A0-E0, D0-A100-E0, and D-50-A50-E0 to provide additional insight into their structural features. As with the AFM results, the membranes containing hydrogen bond donor and acceptor showed similar features to the control membrane (see Figure S8). All membranes imaged with SAXS exhibited broad scattering peaks, indicating an amorphous structure consistent with that observed in other polymer AEMs.[43]

Thus, although we found evidence of phase separation within our membranes, their micro- and nanostructure did not appear to change significantly or systematically compared to the control membrane when hydrogen bond donor or acceptor were present.

3.0 Conclusions

We introduced non-covalent crosslinks comprising hydrogen bond donor-acceptor pairs into anion exchange membrane polymers and evaluated their effects on membrane properties. We found that non-covalent crosslinking enables a degree of independent control over permselectivity and conductivity that is usually not available in conventional, covalently-crosslinked membranes. Specifically, we found that:

- Hydrogen bond donor (methacrylic acid, MAAc) reduced water uptake and increased permselectivity relative to the control membrane, without affecting conductivity.
- Hydrogen bond acceptor (dimethylacrylamide DMAA) increased water uptake and conductivity without substantially reducing permselectivity.
- The combined inclusion of donor (MAAc) and acceptor (DMAA) improved both permselectivity and conductivity simultaneously, escaping the tradeoff relationship typically observed in covalently-crosslinked membranes.
- The combined effects of MAAc and DMAA were not additive (i.e., not easily predictable based on their individual effects), suggesting that they interact with one another inside the membrane.
- The exact mechanism by which hydrogen bond donors and acceptors affect membrane permselectivity and conductivity remains unclear. However, it does not appear that MAAc or DMAA caused significant changes to the membrane's micro- or nanostructure.
- Based on the exciting prospect of independently tunable permselectivity and conductivity, we believe the behavior of non-covalent crosslinks in ion exchange membranes merits further study.

4.0 Experimental

4.1 Materials

Membranes in this study were synthesized from commercially available materials. [2-(Methacryloyloxy)ethyl]trimethylammonium chloride (MAOTMAC, cationic monomer, 75% solution in water), poly(ethylene glycol) diacrylate (PEGDA, covalent crosslinker, average M_n=250 g.mol^{-1}), methyl methacrylate (MMA, neutral ester), and 2-Hydroxy-4′-(2-hydroxyethoxy)-2-methylpropiophenone (Irgacure 2959, photoinitiator) were purchased from Sigma-Aldrich. Methacrylic acid (MAAc, hydrogen bond donor) and N,N-dimethylacrylamide (DMAA, hydrogen bond acceptor) were purchased from Fisher Scientific. Laboratory grade water (LGW, >18 MΩ.cm), ethanol, and 1-propanol were used as solvents. All materials were used without further purification.

4.2 Membrane Synthesis

Freestanding membranes were prepared by photoinitiated free radical polymerization of mixtures containing solvent (ethanol), positively charged monomer (MAOTMAC), covalent crosslinker (PEGDA), neutral ester (MMA), non-covalent crosslinkers (MAAc as hydrogen bond donor and/or DMAA as hydrogen bond acceptor), and photoinitiator (IrgaCure 2959). The chosen amounts of each component were combined into a single glass vial and stirred at 500 rpm on a hot plate set to 50 °C. To facilitate dispensing small quantities, IrgaCure was added to the mixture from a 50 mg.mL^{-1} stock solution in 1-propanol. The initiator concentration in all cases was 0.05 wt%. After the pre-polymerization mixture became optically transparent (i.e. all components were fully dissolved) we dispensed 1.3 mL onto the surface of a clear borosilicate glass plate coated with a hydrophobic silane coupling agent (Rain-X, Illinois Tool Works, Houston, TX). Stainless steel spacers (nominal thickness = 127 μm) were placed on the edges of

the glass, and another glass plate identical to the first was placed on top. This arrangement sandwiched the liquid pre-polymerization mixture between the glass plates, creating a film with a thickness defined by the stainless-steel spacers. The plates were fastened together with clips and exposed to medium-wavelength ultraviolet light delivered by five UVP 34004201 bulbs (nominal peak output at 302 nm). We cured the membranes for a total of 30 minutes, flipping the plates over every 7.5 minutes to ensure equal exposure of the top and bottom surfaces to the UV light. After curing, we carefully separated the glass plates and removed the membrane. Samples from each film were cut for analysis of the gel fraction (see below), and the remainder of the membrane was immediately placed in LGW. Prior to any further testing, membranes were equilibrated in LGW for at least 48 h, during which the water was replaced twice to remove any unreacted monomers and residual solvents.

Table 1. Molar composition of pre-polymerization mixtures used to synthesize membranes in this work.

Sample	Theoretical IEC ($meq.g^{-1}$)	% of Y that is Donor or Acceptor	PEGDA[a] (X) (mol x 2)	MMA[a] (Y) (E, mol)	MAAc[a] (Y) (D, mol)	DMAA[a] (Y) (A, mol)	MAOTMAC[a] (Z) (mol)	Total monomer concentration[b] before polymerization (wt%)	Gel Fraction (%)
Control membrane									
D0-A0-E100	2.18	0	1.2	1	0	0	1	73%	86% ± <1%
Membranes containing donor without acceptor									
D50-A0-E50	2.22	50%	1.2	0.5	0.5	0	1	73%	82% ± <1%
D100-A0-E0	2.25	100%	1.2	0	1.0	0	1	73%	83% ± <1%
Membranes containing acceptor without donor									
D0-A50-E50	2.19	50%	1.2	0.5	0	0.5	1	73%	85% ± <1%
D0-A100-E0	2.19	100%	1.2	0	0	1.0	1	73%	85% ± 1%
Membranes containing both donor and acceptor									
D13-A13-E74	2.19	25%	1.2	0.75	0.125	0.125	1	73%	84% ± 1%
D25-A25-E50	2.20	50%	1.2	0.5	0.25	0.25	1	73%	82% ± 3%
D38-A38-E24	2.21	75%	1.2	0.25	0.375	0.375	1	73%	84% ± <1%
D50-A50-E0	2.22	100%	1.2	0	0.5	0.5	1	73%	84% ± 1%
D25-A75-E0	2.20	100%	1.2	0	0.25	0.75	1	73%	83% ± <1%
D75-A25-E0	2.24	100%	1.2	0	0.75	0.25	1	73%	81% ± <1%

[a] PEGDA is the covalent crosslinker, MMA is the neutral ester, MAAc is the hydrogen bond donor, DMAA is the hydrogen bond acceptor, and MAOTMAC is the cationic monomer. The moles of PEGDA listed in the table represent moles of polymerizable groups. Since PEGDA is difunctional, the values listed are 2x the number of moles of PEGDA molecules in the pre-polymerization mixture.
[b] "Total monomer concentration" refers to the combined concentration of PEGDA, MMA, MAAc, DMAA, and MAOTMAC. The remaining 27% is accounted for by the solvent.

4.3 Gel fraction

To confirm that the monomers reacted to form a crosslinked network, we estimated the gel fraction of the membranes, after Tran et al.[50] The unhydrated sample of each film cut immediately after curing was dried in an incubator at 65 °C for 48 hr to remove residual solvent, and then weighed. Next, it was equilibrated in DI water for at least 48 hr (replacing the water twice) to extract any unreacted monomer. The sample was dried at 65 °C for 48 hr and weighed again. We calculated the gel fraction as the weight after extracting unreacted monomer divided by the weight of the sample before extraction.

4.4 Water uptake

Water uptake (i.e., swelling degree) of the membranes was measured gravimetrically.[53] After removing unreacted monomers by soaking in LGW as described in Section 4.2, membrane coupons were equilibrated in 0.5 M sodium chloride for 24 h, then blotted dry with a laboratory wipe[16,54] and weighed using an analytical balance. Membrane coupons were subsequently dried in an incubator at 65 °C for 48 h[55] and then weighed again. The water uptake (w_u, g H_2O per g dry polymer) was calculated from the wet and dry masses (m_{wet} and m_{dry}, respectively) as[53,56]

$$w_u = \frac{m_{wet} - m_{dry}}{m_{dry}} \quad . \tag{1}$$

We report the average and standard error of at least five replicate SD measurements.

4.5 Permselectivity

The preferential transport of counter-ions was quantified by the membrane permselectivity, which we measured using a technique similar to that described in our previous work.[57] Briefly, membrane coupons were installed in a two-compartment cell (volume of each compartment = 17

mL, open area=7.065 cm^2) containing Ag/AgCl wire reference electrodes. Prior to each experiment, reservoirs connected to the respective cell compartments were filled with 500 mL of either 0.5 M or 0.1 M sodium chloride solution. These solutions were circulated through the cell at a flow rate of approximately 4 $mL.min^{-1}$ using a peristaltic pump. A potentiostat (VMP3, Bio-Logic) was used to record the potential difference between the reference electrodes until a stable reading was obtained. The measured potential difference was corrected for electrode offset potentials, as described previously,[57] to obtain the membrane potential, E_{mem} (mV). E_{mem} was used to calculate the apparent permselectivity, α (dimensionless) as

$$\alpha = \frac{\frac{E_{mem}}{E_{mem,ideal}} + 1 - 2t_{ct}}{2t_{co}} \quad , \qquad (2)$$

where $E_{mem,ideal}$ (37.9 mV at room temperature) is the potential of an ideally selective membrane separating 0.5 M and 0.1 M sodium chloride solution calculated according to the Nernst equation, t_{ct} (0.604, dimensionless) and t_{co} (0.396, dimensionless) are the transport numbers of the counter-ion (Cl^-) and co-ion (Na^+), respectively. We report the average and standard error of replicate measurements conducted on at least five different membrane coupons.

4.6 Conductivity

Membrane conductivity was obtained from membrane resistance and thickness measurements. Membrane coupons were installed in the same two-compartment cell described in Section 4.5, but this time the cell contained platinized titanium working and counter electrodes and single-junction Ag/AgCl reference electrodes (BaSi, Inc. RE-5B) installed in fine-tipped Luggin capillaries. Cell compartments were filled with 0.5 M sodium chloride, which was circulated through both compartments for the duration of the measurement. A potentiostat (VMP3, Bio-

logic) was used to perform galvanostatic electrochemical impedance spectroscopy (GEIS) over a frequency range of 1-1000 Hz with an amplitude of 1 mA. The combined ohmic resistance of the membrane and solution was determined from the high frequency intercept of the Nyquist plot. The resistance of a "blank" cell (i.e., the measurement cell without a membrane) was subtracted from this value to obtain the membrane resistance, R_{mem} (Ω). Further details of the technique can be found in our previous work.[28] We then used a digital micrometer (L.S. Starrett Co., Athol, MA, model 3732XFL-1) to measure membrane thickness L (μm) in the hydrated state. Membrane resistance was normalized by the membrane area A (7.065 cm^2) and thickness to obtain membrane conductivity, κ_{mem} (mS.cm^{-1}) according to

$$\kappa_{mem} = \frac{L}{AR_{mem}} \frac{1cm}{10^4 \mu m} \quad . \tag{3}$$

We report the average and standard error of at least five replicate measurements, conducted on different membrane coupons.

4.7 Bound water analysis

We estimated the amount of non-freezable or "bound" water in the membranes (i.e., water that is strongly associated with the polymer)[24,50,51] using differential scanning calorimetry (DSC). DSC was performed on hydrated membrane samples (~5 mg) in Tzero aluminum pans with hermetic lids using a TA Instruments DSC2500. Two cool-heat cycles between -100 °C and 30 °C were performed at a rate of 10 °C/min under a nitrogen atmosphere. Samples were loaded at 40 °C. Melt enthalpies of water in the membrane (ΔH_w^m, J.g^{-1}) were calculated by integrating the entire melting enthalpy in the heating curve (including multiple peaks, when present). We calculated the free water content (w_f, g free water per g dry membrane) and bound (non-freezable) water content (w_{nf}, g bound water per g dry membrane) according to[24,51]

$$w_f = \frac{\Delta H_w^m}{\Delta H_w^o}(w_u + 1) \quad , \tag{4}$$

and

$$w_{nf} = w_u - w_{nf} \quad , \tag{5}$$

where ΔH_w^o (333.5 J.g^{-1}) is the enthalpy of melting for pure water, and w_u is the water uptake defined in Section 4.4. We calculated the bound (non-freezable) fraction of total water in the membranes as w_{nf}/w_u .

4.8 FTIR analysis

Fourier transform infrared (FTIR) measurements were collected using a Perkin-Elmer Frontier spectrometer in attenuated total reflection (ATR) mode at a resolution of 1 cm^{-1}. Membrane samples were scanned in the dry state between 4000 and 650 cm^{-1}. Liquid monomers, comonomer mixtures, and pre-polymerization solutions were also scanned to aid in peak identification. For each sample, we report the average of 16 scans. The background signal was measured prior to any sample analysis and was subtracted from each scan automatically. All spectra were baseline corrected and normalized to the range 0-1.

4.9 Atomic Force Microscopy

The microscale morphology of the membrane was probed via phase contrast atomic force microscopy (AFM) using an Asylum Research MFP3D Atomic Force Microscope. This tapping-mode technique responds to differences in the density of the sample associated with differences in composition,[58–62] and hence can detect microscale phase separation. Membranes were analyzed in the wet state after being equilibrated in 0.5 M NaCl solution for at least 24 hr.

4.10 Small angle X-ray scattering (SAXS)

Small angle X-ray scattering (SAXS) was performed at beamline 7.3.3 of the Advanced Light Source (ALS) at Lawrence Berkeley National Laboratory (LBNL). The scattering vector q ranged from 0.005-0.5 $Å^{-1}$, corresponding to nanoscopic feature sizes of approximately 1-100 nm. Membrane samples were imaged while immersed in aqueous salt solutions using cells with X-ray transparent Kapton™ windows, and also in the dry state. Wet membranes were equilibrated in 0.5 M NaCl solutions for at least 24 h prior to imaging, and all images were collected at 25 °C. The background scattering signal due to the Kapton windows was obtained from an empty cell containing ambient air and was subtracted from each sample scattering signal prior to analysis.

Supporting Information

Visual appearance of synthesized membranes; Fourier transform infrared (FTIR) spectra; Conductivity and permselectivity vs. water uptake; Freezable and non-freezable (bound) water analysis; pH-dependent swelling tests; Atomic force microscopy (AFM) images; Small angle X-ray scattering (SAXS) profiles.

Acknowledgement

This work was funded by the University of North Carolina Research Opportunities Initiative (ROI) program, the North Carolina Policy Collaboratory, and the National Institute of Environmental Health Sciences (P42ES031007). Atomic force microscopy was performed at the Chapel Hill Analytical and Nanofabrication Laboratory, CHANL, a member of the North Carolina Research Triangle Nanotechnology Network, RTNN, which is supported by the National Science Foundation, Grant ECCS-2025064, as part of the National Nanotechnology Coordinated Infrastructure, NNCI. R. Kingsbury was supported by the National Science

Foundation Graduate Research Fellowship Program under Grant No. DGE-1144081. Any opinions, findings, and conclusions or recommendations expressed in this material are those of the authors and do not necessarily reflect the views of the National Science Foundation.

References

(1) Tanaka, Y. *Ion Exchange Membranes: Fundamentals and Applications*; Tanaka, Y., Ed.; Elsevier: Amsterdam, 2007.

(2) Jiang, C.; Hossain, M.; Li, Y.; Wang, Y.; Xu, T. Ion Exchange Membranes for Electrodialysis : A Comprehensive Review of Recent Advances. *J. Membr. Sep. Technol.* **2014**, *3*, 185–205.

(3) Alotto, P.; Guarnieri, M.; Moro, F. Redox Flow Batteries for the Storage of Renewable Energy: A Review. *Renew. Sustain. Energy Rev.* **2014**, *29*, 325–335. https://doi.org/10.1016/j.rser.2013.08.001.

(4) Luo, T.; Abdu, S.; Wessling, M. Selectivity of Ion Exchange Membranes: A Review. *J. Membr. Sci.* **2018**, *555* (March), 429–454. https://doi.org/10.1016/j.memsci.2018.03.051.

(5) Mei, Y.; Tang, C. Y. Recent Developments and Future Perspectives of Reverse Electrodialysis Technology: A Review. *Desalination* **2017**, *425* (September 2017), 156–174. https://doi.org/10.1016/j.desal.2017.10.021.

(6) He, G.; Li, Z.; Zhao, J.; Wang, S.; Wu, H.; Guiver, M. D.; Jiang, Z. Nanostructured Ion-Exchange Membranes for Fuel Cells: Recent Advances and Perspectives. *Adv. Mater.* **2015**, *27* (36), 5280–5295. https://doi.org/10.1002/adma.201501406.

(7) Sata, T. *Ion Exchange Membranes: Preparation, Characterization, Modification, and Application*; Royal Society of Chemistry: Cambridge, 2004.

(8) Xu, T. Ion Exchange Membranes: State of Their Development and Perspective. *J. Membr. Sci.* **2005**, *263* (1–2), 1–29. https://doi.org/10.1016/j.memsci.2005.05.002.

(9) Kamcev, J.; Freeman, B. D. Charged Polymer Membranes for Environmental/Energy Applications. *Annu. Rev. Chem. Biomol. Eng.* **2016**, *7* (1), 111–133. https://doi.org/10.1146/annurev-chembioeng-080615-033533.

(10) Długołęçki, P.; Nijmeijer, K.; Metz, S. J.; Wessling, M. Current Status of Ion Exchange Membranes for Power Generation from Salinity Gradients. *J. Membr. Sci.* **2008**, *319* (1–2), 214–222. https://doi.org/10.1016/j.memsci.2008.03.037.

(11) Hong, J. G.; Zhang, B.; Glabman, S.; Uzal, N.; Dou, X.; Zhang, H.; Wei, X.; Chen, Y. Potential Ion Exchange Membranes and System Performance in Reverse Electrodialysis for Power Generation : A Review. *J. Membr. Sci.* **2015**, *486*, 71–88.

(12) Yan, X.; Zheng, W.; Ruan, X.; Pan, Y.; Wu, X.; He, G. The Control and Optimization of Macro/Micro-Structure of Ion Conductive Membranes for Energy Conversion and Storage. *Chin. J. Chem. Eng.* **2016**, *24* (5), 558–571. https://doi.org/10.1016/j.cjche.2016.03.003.

(13) Geise, G. M.; Paul, D. R.; Freeman, B. D. Fundamental Water and Salt Transport Properties of Polymeric Materials. *Prog. Polym. Sci.* **2014**, *39* (1), 1–42. https://doi.org/10.1016/j.progpolymsci.2013.07.001.

(14) Fan, H.; Yip, N. Y. Elucidating Conductivity-Permselectivity Tradeoffs in Electrodialysis and Reverse Electrodialysis by Structure-Property Analysis of Ion-Exchange Membranes. *J. Membr. Sci.* **2019**, *573*, 668–681. https://doi.org/10.1016/j.memsci.2018.11.045.
(15) Russell, S. T.; Pereira, R.; Vardner, J. T.; Jones, G. N.; Dimarco, C.; West, A. C.; Kumar, S. K. Hydration Effects on the Permselectivity-Conductivity Trade-Off in Polymer Electrolytes. *Macromolecules* **2020**, *53* (3), 1014–1023. https://doi.org/10.1021/acs.macromol.9b02291.
(16) Geise, G. M.; Hickner, M. a.; Logan, B. E. Ionic Resistance and Permselectivity Tradeoffs in Anion Exchange Membranes. *ACS Appl. Mater. Interfaces* **2013**, *5*, 10294–10301. https://doi.org/10.1021/am403207w.
(17) Liu, Y.; Tang, Z.; Wu, S.; Guo, B. Integrating Sacrificial Bonds into Dynamic Covalent Networks toward Mechanically Robust and Malleable Elastomers. *ACS Macro Lett.* **2019**, *8* (2), 193–199. https://doi.org/10.1021/acsmacrolett.9b00012.
(18) Sun, T. L.; Kurokawa, T.; Kuroda, S.; Ihsan, A. Bin; Akasaki, T.; Sato, K.; Haque, M. A.; Nakajima, T.; Gong, J. P. Physical Hydrogels Composed of Polyampholytes Demonstrate High Toughness and Viscoelasticity. *Nat. Mater.* **2013**, *12* (10), 932–937. https://doi.org/10.1038/nmat3713.
(19) Sun, T. L.; Cui, K.; Gong, J. P. Tough, Self-Recovery and Self-Healing Polyampholyte Hydrogels. *Polym. Sci. Ser. C* **2017**, *59* (1), 11–17. https://doi.org/10.1134/s1811238217010118.
(20) Li, G.; Song, Y.; Liu, Y.; Qi, T. Towards Dynamic, but Supertough Healable Polymers via Biomimetic Hierarchical Hydrogen Bonding Interaction. *Angew. Chem.* **2018**, 1–6. https://doi.org/10.1002/ange.201807622.
(21) Hu, X.; Vatankhah-Varnoosfaderani, M.; Zhou, J.; Li, Q.; Sheiko, S. S. Weak Hydrogen Bonding Enables Hard, Strong, Tough, and Elastic Hydrogels. *Adv. Mater.* **2015**, *27* (43), 6899–6905. https://doi.org/10.1002/adma.201503724.
(22) Schmidt-Rohr, K.; Chen, Q. Parallel Cylindrical Water Nanochannels in Nafion Fuel-Cell Membranes. *Nat. Mater.* **2008**, *7*, 75–83. https://doi.org/10.1038/nmat2074.
(23) Kusoglu, A.; Weber, A. Z. New Insights into Perfluorinated Sulfonic-Acid Ionomers. *Chem. Rev.* **2017**, *117* (3), 987–1104. https://doi.org/10.1021/acs.chemrev.6b00159.
(24) Chang, K.; Luo, H.; Geise, G. M. Water Content, Relative Permittivity, and Ion Sorption Properties of Polymers for Membrane Desalination. *J. Membr. Sci.* **2019**, *574* (August 2018), 24–32. https://doi.org/10.1016/j.memsci.2018.12.048.
(25) Smedley, S. B. WATER HYDROGEN BONDING IN PROTON EXCHANGE AND NEUTRAL POLYMER MEMBRANES, Pennsylania State University, 2015.
(26) Epsztein, R.; Shaulsky, E.; Qin, M.; Elimelech, M. Activation Behavior for Ion Permeation in Ion- Exchange Membranes : Role of Ion Dehydration in Selective Transport. *J. Membr. Sci.* **2019**, *1* (203). https://doi.org/10.1016/j.memsci.2019.02.009.
(27) Kwasny, M. T.; Zhu, L.; Hickner, M. A.; Tew, G. N. Thermodynamics of Counterion Release Is Critical for Anion Exchange Membrane Conductivity. *J. Am. Chem. Soc.* **2018**, *140*, 7961–7969. https://doi.org/10.1021/jacs.8b03979.
(28) Zhu, S.; Kingsbury, R. S.; Call, D. F.; Coronell, O. Impact of Solution Composition on the Resistance of Ion Exchange Membranes. *J. Membr. Sci.* **2018**, *554*, 39–47. https://doi.org/10.1016/j.memsci.2018.02.050.

(29) Shaposhnik, V. A.; Butyrskaya, E. V. Computer Simulation of Cation-Exchange Membrane Structure: An Elementary Act of Hydrated Ion Transport. *Russ. J. Electrochem.* **2004**, *40* (7), 767–770. https://doi.org/10.1023/B:RUEL.0000035263.28700.ce.
(30) Badessa, T.; Shaposhnik, V. The Electrodialysis of Electrolyte Solutions of Multi-Charged Cations. *J. Membr. Sci.* **2016**, *498*, 86–93. https://doi.org/10.1016/j.memsci.2015.09.017.
(31) Smedley, S. B.; Chang, Y.; Bae, C.; Hickner, M. A. Measuring Water Hydrogen Bonding Distributions in Proton Exchange Membranes Using Linear Fourier Transform Infrared Spectroscopy. *Solid State Ion.* **2015**, *275*, 66–70. https://doi.org/10.1016/j.ssi.2015.03.020.
(32) Oyama, H. T.; Tang, W. T.; Frank, C. W. Effect of Hydrophobic Interaction in the Poly(Methacrylic Acid)/Poly(Ethylene Glycol) Complex. *Macromolecules* **1987**, *20*, 1839–1847. https://doi.org/10.1021/ma00174a024.
(33) Wang, Y.; Morawetz, H. Fluorescence Study of the Complexation of Poly(Acrylic Acid) with Poly(N,N-Dimethylacrylamide-Co-Acrylamide). *Macromolecules* **1989**, *22* (1), 164–167. https://doi.org/10.1021/ma00191a032.
(34) Kamcev, J.; Paul, D. R.; Freeman, B. D. Effect of Fixed Charge Group Concentration on Equilibrium Ion Sorption in Ion Exchange Membranes. *J Mater Chem A* **2017**, *5* (9), 4638–4650. https://doi.org/10.1039/C6TA07954G.
(35) Kamcev, J.; Paul, D. R.; Freeman, B. D. Equilibrium Ion Partitioning between Aqueous Salt Solutions and Inhomogeneous Ion Exchange Membranes. *Desalination* **2018**, *446* (September), 31–41. https://doi.org/10.1016/j.desal.2018.08.018.
(36) Williams, D. H.; Fleming, I. *Spectroscopic Methods in Organic Chemistry*, 5th ed.; McGraw-Hill, 1995. https://doi.org/10.1038/nrm2275.
(37) Magalhães, A. S. G.; Neto, M. P. A.; Bezerra, M. N.; Ricardo, N. M. P. S.; Feitosa, J. P. A. Application of Ftir in the Determination of Acrylate Content in Poly(Sodium Acrylate-CO-Acrylamide) Superabsorbent Hydrogels. *Quimica Nova* **2012**, *35* (7), 1464–1467. https://doi.org/10.1590/S0100-40422012000700030.
(38) Duran, A.; Soylak, M.; Tuncel, S. A. Poly(Vinyl Pyridine-Poly Ethylene Glycol Methacrylate-Ethylene Glycol Dimethacrylate) Beads for Heavy Metal Removal. *J. Hazard. Mater.* **2008**, *155* (1–2), 114–120. https://doi.org/10.1016/j.jhazmat.2007.11.037.
(39) Bouhamed, H.; Boufi, S.; Magnin, A. Alumina Interaction with AMPS-MPEG Random Copolymers: I. Adsorption and Electrokinetic Behavior. *J. Colloid Interface Sci.* **2003**, *261* (2), 264–272. https://doi.org/10.1016/S0021-9797(03)00100-0.
(40) Shen, Y.; Xi, J.; Qiu, X.; Zhu, W. A New Proton Conducting Membrane Based on Copolymer of Methyl Methacrylate and 2-Acrylamido-2-Methyl-1-Propanesulfonic Acid for Direct Methanol Fuel Cells. *Electrochimica Acta* **2007**, *52* (24), 6956–6961. https://doi.org/10.1016/j.electacta.2007.05.021.
(41) Ye, G.; Lee, J.; Perreault, F.; Elimelech, M. Controlled Architecture of Dual-Functional Block Copolymer Brushes on Thin-Film Composite Membranes for Integrated "Defending" and "Attacking" Strategies against Biofouling. *ACS Appl. Mater. Interfaces* **2015**. https://doi.org/10.1021/acsami.5b06647.
(42) Gobeze, H. B.; Ma, J.; Leonik, F. M.; Kuroda, D. G. Bottom-up Approach to Assess the Molecular Structure of Aqueous Poly(N-isopropylacrylamide) at Room Temperature via Infrared Spectroscopy. *J. Phys. Chem. B* **2020**, *124* (51), 11699–11710. https://doi.org/10.1021/acs.jpcb.0c08424.
(43) Luo, X.; Rojas-Carbonell, S.; Yan, Y.; Kusoglu, A. Structure-Transport Relationships of Poly(Aryl Piperidinium) Anion-Exchange Membranes: Eeffect of Anions and Hydration.

J. Membr. Sci. **2020**, *598* (November 2019). https://doi.org/10.1016/j.memsci.2019.117680.
(44) Coronell, O.; Mariñas, B. J.; Zhang, X.; Cahill, D. G. Quantification of Functional Groups and Modeling of Their Ionization Behavior in the Active Layer of FT30 Reverse Osmosis Membrane. *Environ. Sci. Technol.* **2008**, *42* (14), 5260–5266. https://doi.org/10.1021/es8002712.
(45) Coronell, O.; Gonzalez, M. I.; Marinas, B. J.; Cahill, D. G. Ionization Behavior, Stoichiometry of Association, and Accessibility of Functional Groups in the Active Layers of Reverse Osmosis and Nanofiltration Membranes. *Environ. Sci. Technol.* **2010**, *44* (17), 6808–6814. https://doi.org/10.1021/es100891r.
(46) Coronell, O.; Marinas, B. J.; Cahill, D. G. Accessibility and Ion Exchange Stoichiometry of Ionized Carboxylic Groups in the Active Layer of FT30 Reverse Osmosis Membrane. *Environ. Sci. Technol.* **2009**, *43* (13), 5042–5048. https://doi.org/10.1021/es803595f.
(47) Chen, D.; Werber, J. R.; Zhao, X.; Elimelech, M. A Facile Method to Quantify the Carboxyl Group Areal Density in the Active Layer of Polyamide Thin-Film Composite Membranes. *J. Membr. Sci.* **2017**, *534* (March), 100–108. https://doi.org/10.1016/j.memsci.2017.04.001.
(48) Zhou, X.; Wang, Z.; Epsztein, R.; Zhan, C.; Li, W.; Fortner, J. D.; Pham, T. A.; Kim, J. H.; Elimelech, M. Intrapore Energy Barriers Govern Ion Transport and Selectivity of Desalination Membranes. *Sci. Adv.* **2020**, *6* (48). https://doi.org/10.1126/sciadv.abd9045.
(49) Helfferich, F. *Ion Exchange*; McGraw-Hill: New York, 1962.
(50) Tran, T.; Lin, C.; Chaurasia, S.; Lin, H. Elucidating the Relationship between States of Water and Ion Transport Properties in Hydrated Polymers. *J. Membr. Sci.* **2019**, *574* (December 2018), 299–308. https://doi.org/10.1016/j.memsci.2018.12.059.
(51) Yang, P.; Mather, P. T. *Thermal Analysis to Determine Various Forms of Water Present in Hydrogels*; TA 384; TA Instruments.
(52) Luo, H.; Chang, K.; Bahati, K.; Geise, G. M. Functional Group Configuration Influences Salt Transport in Desalination Membrane Materials. *J. Membr. Sci.* **2019**, *590* (February), 117295. https://doi.org/10.1016/j.memsci.2019.117295.
(53) Güler, E.; Elizen, R.; Vermaas, D. A.; Saakes, M.; Nijmeijer, K. Performance-Determining Membrane Properties in Reverse Electrodialysis. *J. Membr. Sci.* **2013**, *446*, 266–276. https://doi.org/10.1016/j.memsci.2013.06.045.
(54) Geise, G. M.; Cassady, H. J.; Paul, D. R.; Logan, E.; Hickner, M. A. Specific Ion Effects on Membrane Potential and the Permselectivity of Ion Exchange Membranes. *Phys. Chem. Chem. Phys.* **2014**, *16*, 21673–21681. https://doi.org/10.1039/C4CP03076A.
(55) Tanaka, Y. Fundamental Properties of Ion Exchange Membranes. In *Ion Exchange Membranes: Fundamentals and Application*; Elsevier, 2015; pp 29–65. https://doi.org/10.1016/B978-0-444-63319-4.00002-X.
(56) Kingsbury, R. S.; Zhu, S.; Flotron, S.; Coronell, O. Microstructure Determines Water and Salt Permeation in Commercial Ion Exchange Membranes. *ACS Appl. Mater. Interfaces* **2018**, *10* (46), 39745–39756. https://doi.org/10.1021/acsami.8b14494.
(57) Kingsbury, R. S.; Flotron, S.; Zhu, S.; Call, D. F.; Coronell, O. Junction Potentials Bias Measurements of Ion Exchange Membrane Permselectivity. *Environ. Sci. Technol.* **2018**, *52* (8), 4929–4936. https://doi.org/10.1021/acs.est.7b05317.

(58) James, P. J.; Elliott, J. A.; McMaster, J.; Newton, J. M.; Elliott, A. M. S.; Hanna, S.; Miles, M. J. Hydration of Nafion Studied by AFM and X-Ray Scattering. *J. Mater. Sci.* **2000**, *35* (20), 5111–5119. https://doi.org/10.1023/A:1004891917643.
(59) Raghavan, D.; Gu, X.; Nguyen, T.; VanLandingham, M.; Karim, A. Mapping Polymer Heterogeneity Using Atomic Force Microscopy Phase Imaging and Nanoscale Indentation. *Macromolecules* **2000**, *33* (7), 2573–2583. https://doi.org/10.1021/ma991206r.
(60) Khulbe, K. C.; Feng, C. Y.; Matsuura, T. *Synthetic Polymer Membranes: Characterization by Atomic Force Microscopy*; Springer, 2008. https://doi.org/10.1007/978-3-540-73994-4 Library.
(61) Magonov, S. N.; Reneker, D. H. Characterization of Polymer Surfaces With Atomic Force Microscopy. *Annu. Rev. Mater. Sci.* **2002**, *27* (1), 175–222. https://doi.org/10.1146/annurev.matsci.27.1.175.
(62) McLean, R. S.; Sauer, B. B. Tapping-Mode AFM Studies Using Phase Detection for Resolution of Nanophases in Segmented Polyurethanes and Other Block Copolymers. *Macromolecules* **1997**, *30* (26), 8314–8317. https://doi.org/10.1021/ma970350e.